Heat pipe air-cooled thermal management system for lithium-ion batteries: High power applications

Hamidreza Behi [a,b,*], Mohammadreza Behi [c,d], Danial Karimi [a,b], Joris Jaguemont [a,b], Morteza Ghanbarpour [d], Masud Behnia [e], Maitane Berecibar [a,b], Joeri Van Mierlo [a,b]

[a] Research group MOBI – Mobility, Logistics, and Automotive Technology Research Centre, Vrije Universiteit Brussel, Pleinlaan 2, Brussels 1050, Belgium
[b] Flanders Make, Heverlee 3001, Belgium
[c] The University of Sydney, School of Chemical and Biomolecular Engineering, NSW 2006, Australia
[d] Department of Energy Technology, KTH Royal Institute of Technology, SE-10044 Stockholm, Sweden
[e] School of Management, Macquarie University, Sydney, Australia

ARTICLE INFO

ABSTRACT

Thermal management of lithium-ion (Li-ion) batteries in Electrical Vehicles (EVs) is important due to extreme heat generation during fast charging/discharging. In the current study, a sandwiched configuration of the heat pipes cooling system (SHCS) is suggested for the high current discharging of lithium-titanate (LTO) battery cell. The temperature of the LTO cell is experimentally evaluated in the 8C discharging rate by different cooling strategies. Results indicate that the maximum cell temperature in natural convection reaches 56.8 °C. In addition, maximum cell temperature embedded with SCHS for the cooling strategy using natural convection, forced convection for SHCS, and forced convection for cell and SHCS reach 49 °C, 38.8 °C, and 37.8 °C which can reduce the cell temperature by up to 13.7%, 31.6%, and 33.4% respectively. A computational fluid dynamic (CFD) model using COMSOL Multiphysics® is developed and comprehensively validated with experimental results. This model is then employed to investigate the thermal performance of the SHCS under different transient boundary conditions.

1. Introduction

Nowadays, the transportation industry concentrates on clean energy vehicles due to climate change and environmental pollution. Electric vehicles (EVs) and hybrid electric vehicles which produce a smaller amount of carbon dioxide are introduced as a new generation and substitution of the combustion engine-powered vehicles [1]. The rechargeable battery is regarded as an optimum energy storage device and driving power. Among all kinds of batteries, lithium-ion (Li-ion) batteries have gained popularity because of their unique features comprising the wide application, high energy, high power density, and long life cycle [2-5]. However, Li-ion batteries are very sensitive to their operating temperature, especially at high C-rates. The C-rate represents the rate of charging/discharging of the cell respect to its maximum capacity. Many researchers have concluded that high temperature affects the charge/discharge efficiency, accelerates the capacity degradation, decreases output power, and reduces the battery life [6-9]. Besides, temperature inhomogeneity distribution in the battery module/pack

increases the inconsistency between cells which leads to the decrease of cycle life. Hence, as it is recommended by researches the optimal working temperature range for Li-ion batteries is 25–40 °C, while the temperature difference in a module is preferred to be preserved below 5 °C [10-12]. Therefore, designing a proper thermal management system (TMS), to preserve the battery temperature within the optimum range and prevent from thermal runaway is vital for the operation of Li-ion batteries [13,14]. Many active, passive, and hybrid cooling systems have been developed for electric vehicles and electronic cooling. Up to the present time, different kinds of TMSs like air cooling, liquid cooling, and passive cooling based on phase change material (PCM) have been widely used [15–22,80,81]. The air cooling system is extensively used because of its advantages in terms of simple structure, low cost, and lightweight. Many studies have been done to improve the cooling performance of the air cooling system by structure design, battery layout, and control strategy [23-26]. Nevertheless, due to the low specific heat of air, under stressful operating conditions, a considerable temperature difference can easily occur in a battery module/pack [27,28]. Liquid cooling is a more effective cooling system as the liquid coolant has a

Nomenclature

Δt	Time Interval (t)	k_{eff}	Effective Thermal Conductivity of the Heat pipe (W/m.K)
T	Battery Temperature (K)	Q_{hp}	Heat Transferred by Heat pipe (W)
I	Discharge Current (Ah)	A_h	The cross-section of the Heat pipe (m^2)
V	Operating Voltage (V)	q_g	Cell Heat Generation (W)
v	Velocity (m/s)	V	Volume (m^3)
m	Mass of the Cell (kg)		
c_p	Specific Heat Capacity (J/kg.K)	*Greek*	
T_{amb}	Temperature of Ambient (K)	$\rho^{'}$	Resistivity (k/W)
R_{bt}	Total Resistance of the Battery (K/W)	ρ	Density (kg/m^3)
R_{tab}	Total Resistance of the Battery Tab (K/W)	*Acronyms*	
k	Thermal Conductivity (W/m.K)	*Li-ion*	Lithium-ion
$k_{T,x,y,z}$	Thermal Conductivity in x,y and z Axis (W/m.K)	EVs	Electrical Vehicles
p	Pressure (Pa)	CFD	Computational Fluid Dynamics
S	Cross-section of the Tab and Cell (m^2)	*TMS*	Thermal Management System
h	Heat Transfer Coefficient (W/m^2.K)	*SHCS*	Sandwiched Heat pipes Cooling System
q_{conv}	Free Cooling Heat Transfer (W)	SOC	State of Charge
Q_{Cell}	Power Loss of Battery (W)	LTO	lithium-titanate
g_i	Gravity (m/s^2)	*PCM*	Phase Change Material
		3D	3-Dimentional

much higher heat transfer of coefficient. Several studies have been focused on the flow channel design and thermal properties of coolant [29-32]. However, using liquid as a coolant can cause leakage and short circuit. Moreover, using components like pipes and pumps increase the cost of the system. Besides, the high-pressure drop across the liquid-cooled heat exchangers cause extra energy consumption [33]. On the other hand, passive methods such as PCM and Nano-PCMs have gained more attention in recent years [34-36]. PCM can successfully decrease the average temperature and provide a uniform temperature distribution for the Li-ion battery module/pack [37-39]. Nevertheless, high cost, lack of thermal stability for a long time, low thermal conductivity, and leaking problem after melting has not been completely solved [40-42]. Recently, heat pipe cooling technology has been used in many industrial applications [43-46]. Heat pipes are well-known as thermal superconductors that their thermal conductivity reaches up to 90 times more than a copper bar with the same dimension [47]. Heat pipes are classified as passive cooling systems that have many advantages including low cost, high heat transfer performance, and efficiency [44,48]. Heat pipes have flexible geometry and are classified into traditional circular pipes, long flat pipes, and the plate heat pipes, which have a compact structure and

long service life. The tubular heat pipes received the attention of the researchers in many studies. However, one of the key issues is the limitation of the contact area between the heat pipe and the heat source [49]. Therefore, the flat heat pipes and flat loop heat pipes are frequently used with the purpose of thermal contact increase. Behi et al. [50] presented an experimental and numerical study using the L shaped flat heat pipe as a novel TMS for cylindrical battery module. Dan et al. [51] numerically designed a thermal management system equipped with a micro heat pipe array. They proved that the micro heat pipe array TMS could provide a quick response for temperature stability during the rapidly changing operating condition. Ye et al. [52] experimentally designed a micro heat pipe arrays for the charging/discharging cycle. They found that the proposed cooling system could operate well and decrease the temperature and temperature difference effectively. Ye et al. [53] numerically improved heat pipe TMS for fast-charging Li-ion battery cell/pack. They proved experimentally and numerically, that heat pipe TMS is capable for thermal management of batteries. Tran et al. [54] experimentally considered the cooling effect of the flat heat pipe and conventional heat sink. They discovered that heat pipes can decrease thermal resistance and keep the batteries at a safe temperature.
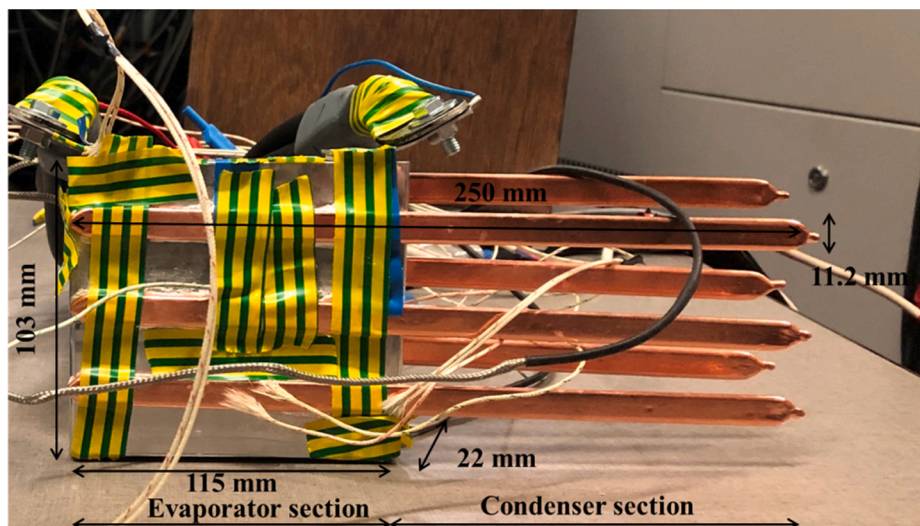

Fig. 1. The LTO prismatic cell and SHCS with their dimensions.

Table 1

The main properties of the heat pipe and battery cell.

Parameter (Heat pipe)	Value	Parameter (Battery cell)	Value
Heat pipe length (mm)	250	Chemistry	LTO
Dimension L × W (mm)	11.2 × 3.5	Shape	Prismatic
Working fluid	Distilled water	Nominal Voltage (V)	2.3
Wick structure	Sintered	Maximum voltage (V)	2.7
Thermal conductivity (W/m.K)	8212	Dimensions L × W × H (mm)	115 × 22 × 103
Cooling Power (W)	100	Capacity (Ah)	23
Operation temperature (℃)	30–120	Heat specific capacity (J/kg.K)	1150
Cross-section area (mm^2)	38.32	Thermal conductivity x, y,z (W/m.K)	31, 0.8, 31
L$_{eff}$(mm)	125	Weight (kg)	0.550

Thermal behavior and simulation of the battery cell can play an important role in cell temperature monitoring. Generally, an accurate validation process of the thermal model can be difficult and challenging. Comparing the experimental measurements from the cell surface temperature with a simulation model is a less complex and faster method of model validation [55]. Nonetheless, owing to the intricacy of electrochemical reactions and divers current density distribution inside the cell, the 3-Dimentional (3D) distribution of cell surface temperature can be non-uniform especially, for large rectangular shaped cells in automotive applications [56-60]. Also, according to the type of applied load profile, the location of maximum and average temperature can be different on the surface of the cell [61]. This temperature inhomogeneity makes more challenging TMS for the battery cell in order to maintain a uniform temperature inside the battery module/pack during charging/discharging. Therefore, designing a sophisticated and capable cooling system is necessary.

In the current study, cooling technology using heat pipes and air cooling is investigated. Surface temperature histories and temperature gradients of the LTO cell are collected experimentally and compared with four cooling methods. Moreover, the thermal infrared camera is used to detect and measure the 3D temperature distribution of the cell. For further consideration, the temperature of the cell is measured in the different boundary conditions. The testing results prove that the air cooling system combined heat pipes is an effective TMS to control the temperature variation of Li-ion battery cell with the lowest energy consumption and to improve the performance of the entire battery system. The paper is organized as follows. Section 2 represents the conceptual design of the cooling system. In Section 3, the experimental setup and results are represented. The simulation of the battery cell and its results are described in Section 4. Lastly, a relevant conclusion is drawn in Section 5.

2. Conceptual design of the cooling system

Fig. 1 shows a picture of the sandwiched heat pipes cooling system (SHCS) for a prismatic LTO battery cell with their dimensions. In this design, the cell is sandwiched by six flat heat pipes. The detailed parameters of the battery cell and heat pipes are presented in Table. 1. The SHCS quickly absorb and transfer the heat to the cooling medium (air). Heat pipes are in contact with both sides of the cell, a layer of gap filler with thermal conductivity of 8 W/m.K is applied at the interfaces between the cell and the heat pipes to decrease the thermal contact resistance. The cooling system is designed for the thermal management of the cell during the 8C discharging rate (184 A).

During the discharging process, the heat generated inside the cell and tabs through conduction is transferred by the evaporator sections of the heat pipes to the condenser sections and from there by convection to the circulating air. To test the effect of the cooling system, four scenarios have been considered experimentally as follows:

Considering the transient effect of natural convection on the cell temperature at the 8C discharging rate (NC-Cell).
Investigate the transient effect of natural convection on the cell embedded with SHCS at the 8C discharging rate (NC-Cell-SHCS).
Study the transient effect of natural convection on the cell surface and forced convection on the SHCS at the 8C discharging rate (NC-Cell-FC-SHCS).
Investigate the transient effect of forced convection on the cell embedded with SHCS at the 8C discharging rate (FC-Cell-SHCS).

3. Experimental setup

To design an efficient cooling system with high-temperature uniformity, an LTO prismatic battery cell is embedded with SHCS. The

Fig. 2. The picture of the experimental system (1) Cooling fan; (2) LTO cell and SHCS; (3) PEC® battery tester (4) Personal computer and, Datalogger.
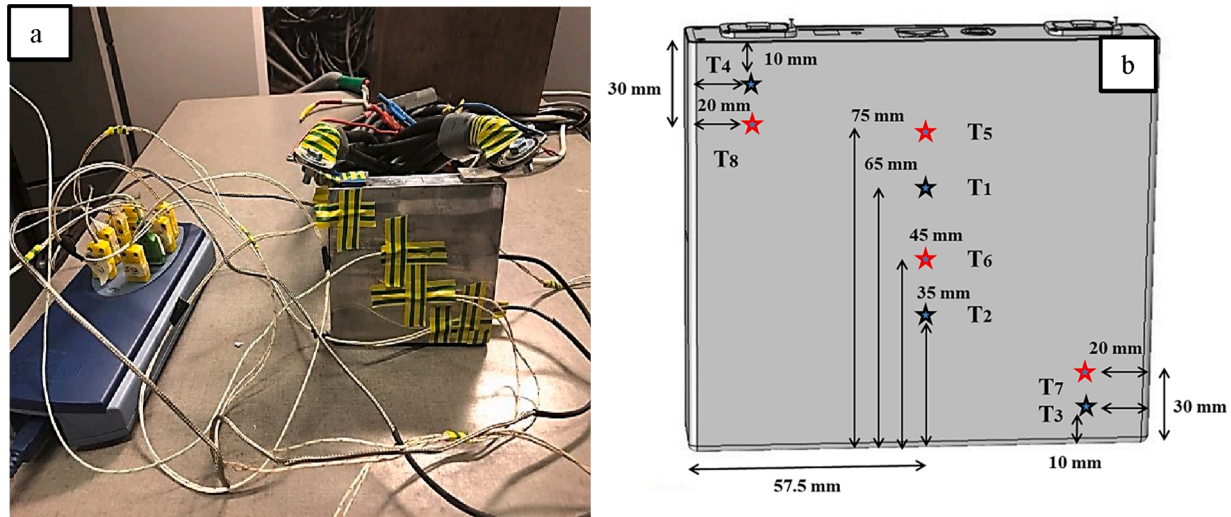
Fig. 3. (a) The picture of the battery cell in presence of natural convection and, (b) the schematic of the cell with the location and dimension of thermocouples of the front (T_1-T_4), backside (T_5-T_8) of the cell.

primary study on a baseline SHCS is conducted as follows. The evaporator sections of six sintered copper heat pipes (with distilled water as the working fluid) are flattened to 3.5 mm in thickness and 115 mm in length. The condenser section of the heat pipe extended with the same thickness and 135 mm length. The experimental setup is built to investigate the performance of SHCS with air cooling for the thermal management of the LTO cell at the 8C discharging rate. The picture of the setup is shown in Fig. 2. The setup comprised a cooling fan, anemometer, LTO cell embedded with SHCS, PEC® battery tester, TC-08 Pico data logger, FLIR thermal camera, eight K-type thermocouples, and a personal computer. All thermocouples connected to the cell are calibrated with an accuracy of ± 0.2 ℃. To cycle the LTO cell, a battery tester is used to obtain the data using a computer linked to the tester. The current and voltage can be monitored using the test bench. Also, the temperature of the cell in 8 points is recorded. To consider the cell temperature evolution under different cooling strategies, the cell is located inside the room with a controlled constant temperature of 22 ℃. The discharging of the cell is carried out in high current by the testers in which the cell is discharged by the current rate of 184 A with a 446 s current profile.

To determine the uncertainty of the experimental tests, the Schultz and Cole [62,63] method have been used.

$$U_R = \left[\sum_{i=1}^{n} \left(\frac{\partial R}{\partial V_I} U_{VI} \right)^2 \right]^{1/2} \qquad (1)$$

where U_{VI} and U_R are the error of every single factor and total errors respectively. The maximum uncertainty is less than 2.01%.

3.1. Experimental result

3.1.1. Natural convection for the LTO cell (NC-Cell)

The natural convection effect using buoyancy-driven convection is the first phase to consider the temperature of the cell. Natural convection is a method that does not consume any energy and regularly is used for electronic cooling applications in which high reliability is important. This characteristic of natural convection is its main advantage. Additionally, this method helps to save the cost, volume, and energy by eliminating the fan. However, natural convection efficiency is low, so improvements are required. Fig. 3a shows the picture of the LTO cell and the location of the eight thermocouples. The natural convection is done at a high discharging current of 184 A from 100% to 0% of the state of charge (SOC) in the ambient temperature of 22 ℃. Besides, Fig. 3b
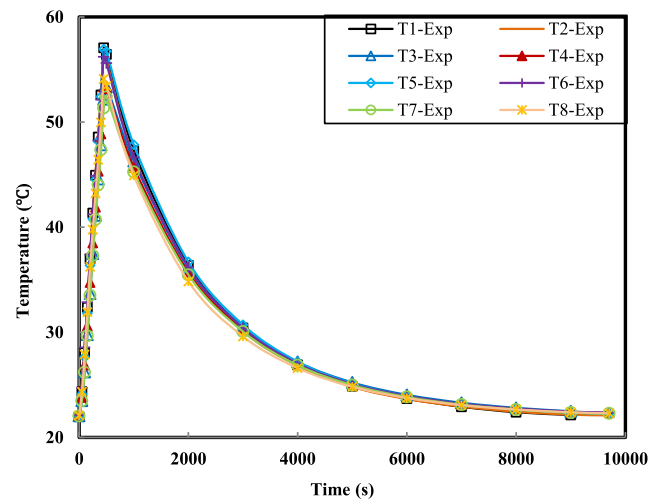

Fig. 4. The temperature variation of the LTO cell in natural convection at an initial temperature of 22 ℃ and 8C discharging rate (Exp: Experimental).

illustrates the schematic location and dimension of the thermocouples of T_1-T_8.

The cooling time of the natural convection system for the LTO cell is shown in Fig. 4. In the first scenario, the LTO cell is discharged at 8C to reach the highest temperature, and the cell temperature is recording when the discharge stops until the cell reaches to the initial temperature. As can be seen, the temperatures of thermocouples in the center and top of the cell (T_1, T_2, T_5, T_6) are higher and reach almost 55–57 ℃. The temperatures of thermocouples in edges of the cell (T_3, T_4, T_7, T_8) with the same trend reach almost 52–53 ℃ which shows the temperature in the center and top of the cell is higher. As shown, according to the low heat transfer coefficient of air and low heat dissipation, the maximum temperature of the cell through natural convection takes 9700 s to decrease to 22 ℃.

3.1.1.1. Thermal image analysis of natural convection.
Fig. 5 shows the thermal images of the 3D-thermal distribution of the cell surface temperature during discharge at 184 A. To achieve precise results from the thermal camera, the cell is placed in a dark and constant temperature environment. Additionally, the cell surfaces are painted homogeneously with dull black paint to decrease the consequence of visible light
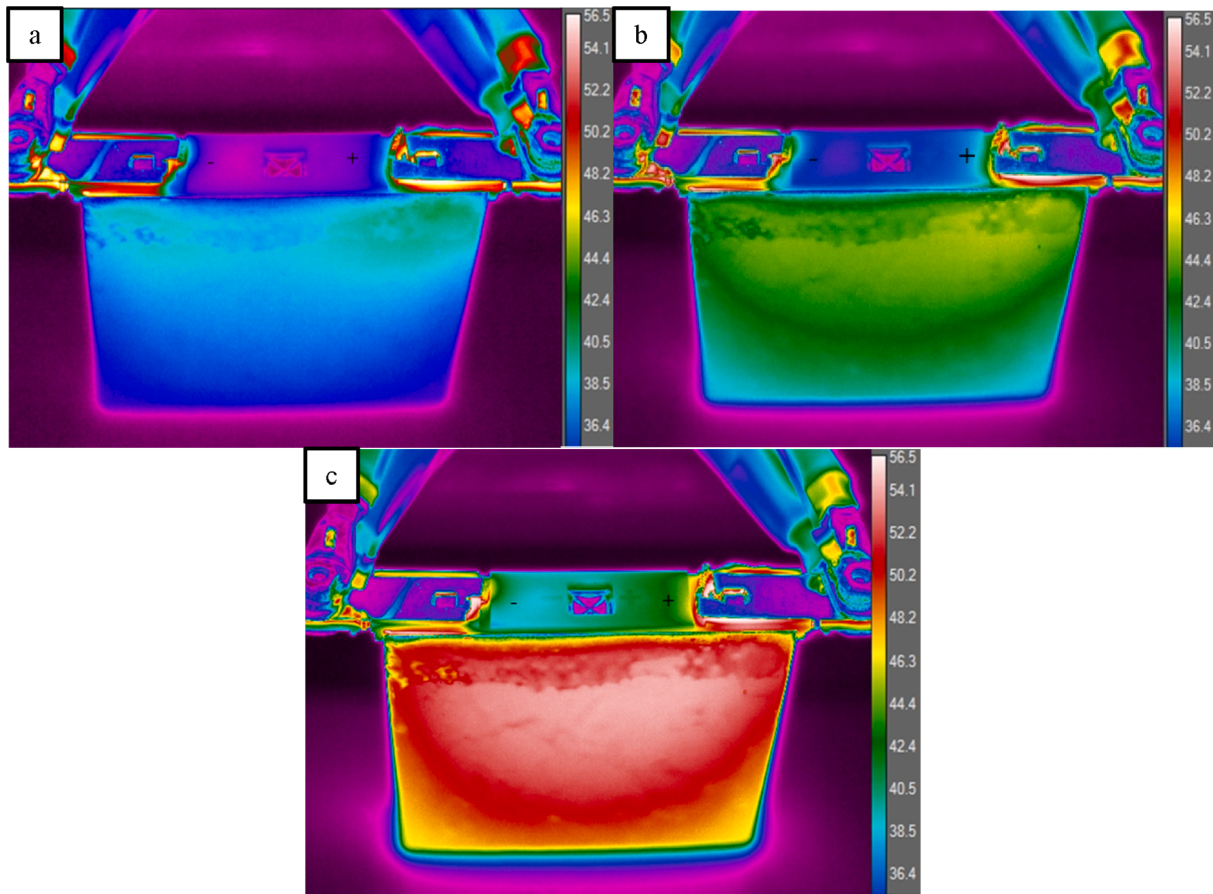
Fig. 5. The infrared picture of LTO cell at (a) 200 s, (b) 350 s and (c) 446 s of the 8C discharging (184 A) rate in the presence of natural convection.

reflections. The FLIR thermal camera is calibrated within the temperature range of 0–120 °C, with a maximum error of 2% by the manufacturer. As can be seen from the temperature distribution pattern of the thermal images at 200 s firstly, the hottest area happens in the adjacent region of the tabs of the cell and a little higher near the positive tab. The higher temperature in the positive tab is related to the comparatively higher resistance of the aluminum positive tab and current collector compared with the copper in the negative tab [64,65]. However, as the discharging process continues (Fig. 5b) and at the end (Fig. 5c), the temperature distribution becomes more uniform over the whole surface of the cell, with the hottest area located in the center and top of the cell. According to Fig. 5 the maximum temperature for 200 s, 350 s, and 446 s reach 39 °C, 48 °C, and 56 °C respectively.

3.1.2. Natural convection for the cell and SHCS (NC-Cell-SHCS)

In the second experimental scenario, the SHCS is used to dissipate heat from the LTO cell under the natural convection. Fig. 6a shows the picture of LTO cell and SHCS with the location of the eight thermocouples. Like the first scenario, the natural convection was done at an 8C discharging rate with a current of 184 A from 100% to 0% of SOC in the ambient temperature of 22 °C. Fig. 6b shows the schematic front and backside of the cell with the location and dimension of the thermocouples of T_1-T_8.

Fig. 7 shows the effect of the natural convection and total cooling time of the test when the cell is embedded with the SHCS. The surface temperatures of the cell are recorded by T_1-T_8 thermocouples as it is depicted in Fig. 7b. Explicitly, the SHCS has a relatively appropriate effect on the temperature of the cell. The thermocouples of T_1, T_2, T_5, and T_6 reach almost 48–49 °C and the temperatures of thermocouples of T_3, T_4, T_7, and T_8 with the same trend reach almost 43–44 °C which shows a 13.7% temperature reduction compare with the first scenario.

The SHCS continuously absorbs and transfers the heat to the cooling medium (air). The maximum temperature of the cell embedded with SHCS through natural convection takes 7000 s to decrease to 22 °C which shows about a 30% reduction in total time compares with cell in natural convection cooling. However, the optimal temperature range for Li-ion is 25–40 °C [12]. Therefore, the cell temperature is greater than its optimal operating temperature range which proves the usage of forced convection.

3.1.3. Natural convection for the cell and forced convection for SHCS (NC-Cell-FC-SHCS)

Fig. 8a shows a picture of the battery cell embedded with SHCS in the presence of forced convection and natural convection. In the third scenario, the condenser section of heat pipes is only affected by forced convection with an inlet velocity of 3 m/s. The temperature variation of the cell and the total cooling time of the test are depicted in Fig. 8b. As can be seen clearly, the forced convection has a direct effect on the maximum temperature of the cell. The thermocouples of T_1, T_2, T_5, and T_6 reach almost 37–38 °C and the temperatures of thermocouples of T_3, T_4, T_7, and T_8 with the same trend reach almost 34–35 °C which shows nearly a 31.6% temperature reduction compare with the first scenario. The airflow under forced convection increased the influence of the surface heat transfer coefficient of the cell and heat pipes. The working medium in the evaporator of SHCS can work continuously to transfer the heat generated by the cell to the condenser. The temperature results specify that SHCS combined with forced convection is an ideal solution to reduce the maximum temperature of the cell and improve the temperature uniformity. Moreover, The maximum temperature of the cell embedded with SHCS through the third scenario takes almost 2200 s to decrease to 22 °C which shows a 78% reduction in total time compares with cell in natural convection cooling.
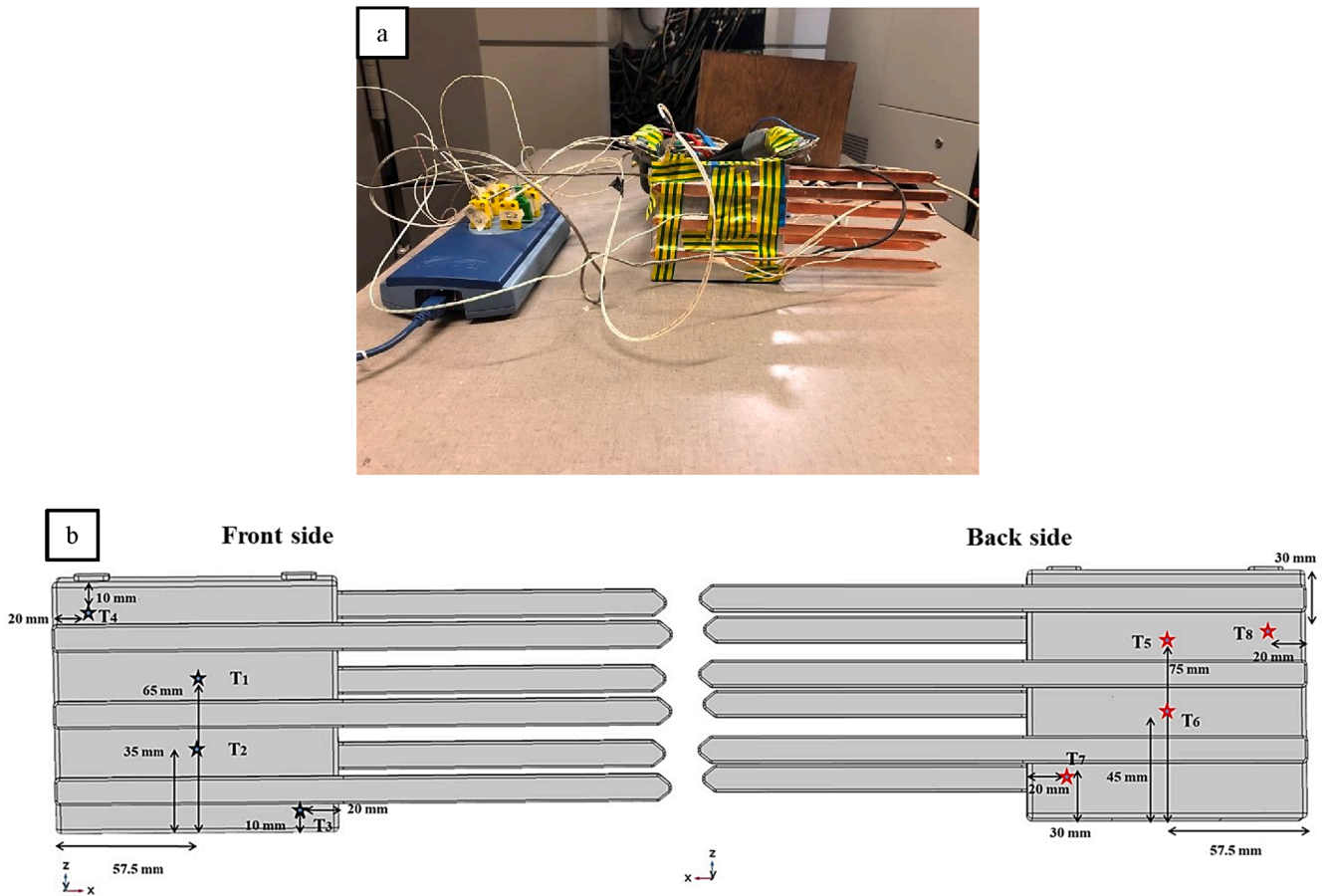
Fig. 6. (a) The picture of the battery cell embedded with SHCS in presence of natural convection and, (b) the schematic of the cell and SHCS with the location and dimension of thermocouples of the front (T_1-T_4) and backside (T_5-T_8) of the cell.
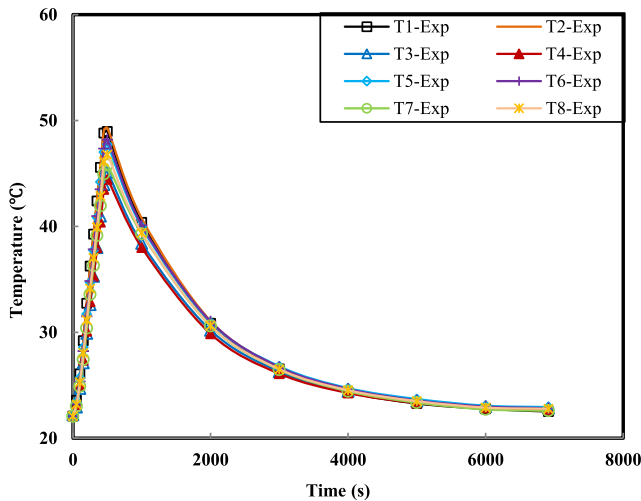

Fig. 7. The temperature variation of the LTO cell embedded with SHCS in natural convection at an initial temperature of 22 °C and 8C discharging rate.

3.1.4. Forced convection for the cell embedded with SHCS (FC- Cell-SHCS)

Fig. 9a indicates a picture of the battery cell embedded with SHCS in the presence of forced convection. In the fourth scenario, the cell, condenser, and evaporator sections of heat pipes are affected by forced convection. The temperature variations of the cell and SHCS with air forced convection under the 8C discharging rate is shown in Fig. 9b. The temperature difference with the third scenario is insignificant. From Fig. 9b, the cells' temperature is controlled in a safe zone (25–40 °C [12]) however, the temperature of thermocouples in airflow direction (T_1-T_4) is lower. The thermocouples of T_1, T_2, T_3, and T_4 reach almost 32–34 °C. Moreover, the temperatures of thermocouples of T_5, T_6, and T_7, T_8 with the same trend reach almost 34 °C and 37 °C respectively which shows approximately a 33.4% temperature reduction compare with natural convection cooling. The results show that the best cooling performance is achieved by the fourth scenario when the forced convection effectively reduces the temperature of the cell. However, the temperature uniformity is lower compared with the third scenario due to the effect of airflow on one side of the cell. As shown in Fig. 9b, the total cooling time is reduced to 1800 s which demonstrates an 82% reduction in total time compares with cell in natural convection cooling.

3.1.5. Maximum temperature variation of the cell in different thermal management scenarios

Fig. 10a shows the maximum temperature variations of the LTO cell under the four thermal management scenarios. At the start of the discharging, there is little difference between the four modes. Over time, the temperature of the cell increased. The maximum temperature under the first scenario reaches 56.8 °C. For the second to fourth scenarios, the maximum temperatures reach 48.7 °C, 36.8 °C and 34.9 °C, respectively. According to Fig. 10b using SHCS has an effective influence on the maximum temperature of the cell. SHCS and forced convection can remove most of the heat generated by the cell at 8C discharging rate and can keep the temperature of the cell in a safe zone temperature, unlike the natural convection.
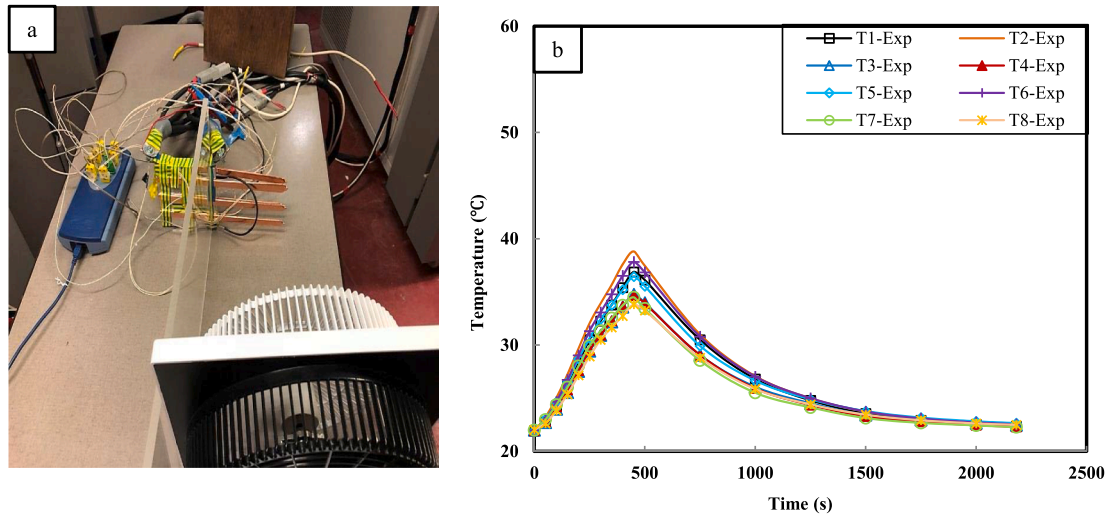
Fig. 8. (a) The picture of the battery cell embedded with SHCS in presence of forced convection and natural convection, (b) the temperature variation of the LTO cell embedded with SHCS in forced convection at an initial temperature of 22 °C and 8C discharging rate.
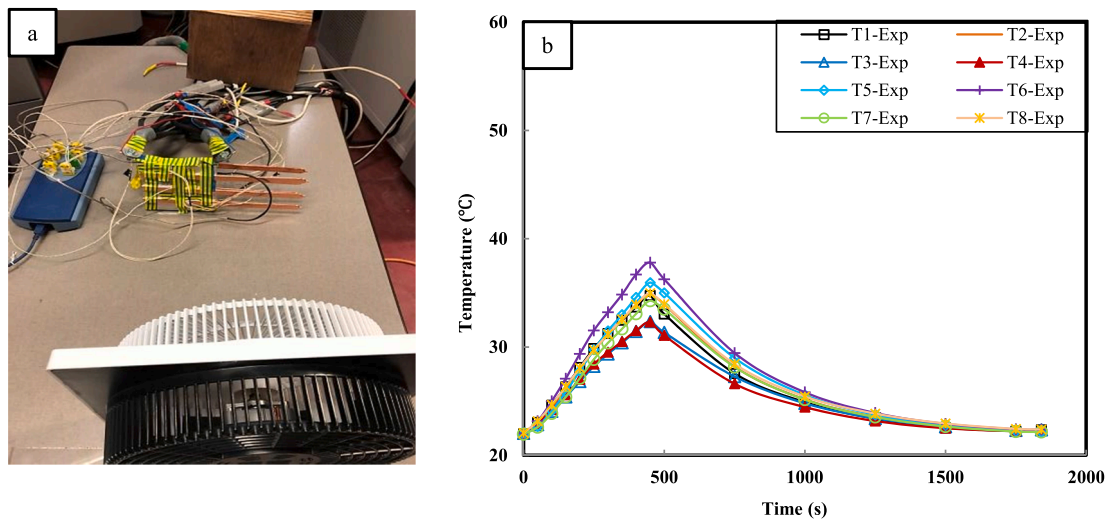

Fig. 9. (a) The picture of the battery cell embedded with SHCS in presence of forced air cooling and, (b) the temperature variation of the LTO cell embedded with SHCS in forced air cooling at an initial temperature of 22 °C and 8C discharging rate.

4. Simulation of the battery model

4.1. Battery thermal modeling

Thermal behavior modeling and simulation of the battery cell can play an important role in cell temperature monitoring. Besides, it can deliver possibilities for the development of battery cells for better thermal management and enhance the thermal safety of the battery module/pack consisting of several cells [66]. The thermal part of the model is connected to the thermodynamics equations for prismatic-shape cells. The simulation process is performed via the CFD commercial software, COMSOL Multiphysics®. The 3D-thermal model has been done by the finite element method to reach the thermal behavior of the cell. Energy equation balance is used to express the transient thermal distribution inside the cell. The cell heat generation to its surrounding is expressed as below [67]:

$$mC_p\frac{\partial T}{\partial t} + q_{loss} = k_x\frac{\partial^2 T}{\partial x^2} + k_y\frac{\partial^2 T}{\partial y^2} + k_z\frac{\partial^2 T}{\partial z^2} + q_g \tag{2}$$

where m, c_p, T, k, and q_g represent the mass, heat capacity, temperature,

thermal conductivity, and heat generation, respectively. Concerning the boundary limits of the model, the heat transfer with the surroundings is determined by the convection equation. Heat transfer convection from the cell to the ambient is calculated as [68]:

$$q_{loss} = q_{Conv} = hA(T_{amb} - T_{bt}) \tag{3}$$

wherein, h and A represent the heat transfer of the coefficient and cross-section area of the cell. Moreover, T_{bt} and T_{amb} show the battery and ambient temperature.

In prismatic shape cell, the thermal conductivities are anisotropic. In fact, along with the battery sheets has a greater value than in the direction normal to the sheets. Equations (4) to (6) represent the thermal conductivity in ×, y, and z-axis. It is necessary to mention that the value of thermal conductivity in different axis is presented in Table 1.

$$k_{T,x} = \frac{\sum L_{i,x} K_{T,i}}{\sum L_{i,x}} \tag{4}$$

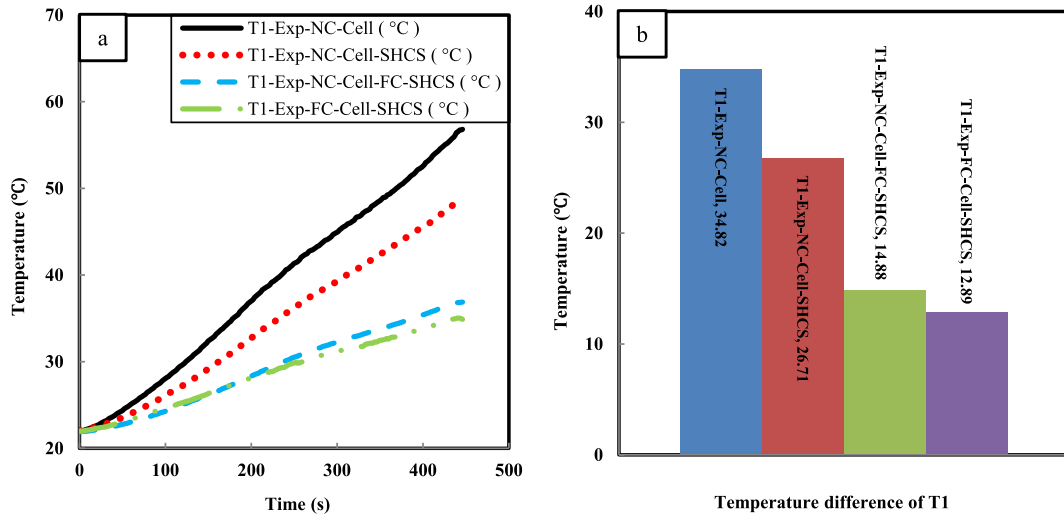$$k_{T,y} = \frac{\sum L_{i,y}}{\sum \frac{L_{i,y}}{K_{T,i,y}}} \tag{5}$$

Fig. 10. (a) The battery surface temperature of T_1 and, (b) the temperature difference of the T_1 in four cooling scenarios at an initial temperature of 22 °C and 8C discharging rate (NC: Natural Convection, FC: Forced Convection).
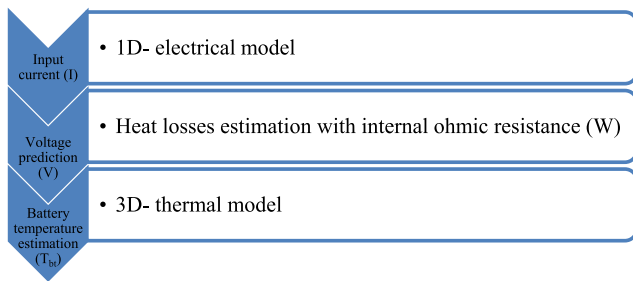

Fig. 11. The thermal modeling methodology and coupling of 1D-3D.

$$k_{T,z} = \frac{\sum L_{i,z} K_{T,i}}{\sum L_{i,z}} \tag{6}$$

In this study, the volumetric heat source is chosen for each domain of the cell. Owing to the non-uniform temperature distribution inside the cell, separated heat sources are used for the cell and tab domains. The value of the heat generation is calculated by considering the ohmic resistance and polarization process. Additionally, equation (8) uses the tab domain [69].

$$q_g = R_{bt}.I^2 + R_1.I_1^2 + R_2.I_2^2 \tag{7}$$

$$\dot{q} = R_{tab}.I^2 \tag{8}$$

$$R_{tab} = \rho^{'} \frac{l}{A} \tag{9}$$

The current and ohmic resistance of the cell shows by I and R_{bt} respectively. According to equation (8) and (9) the R_{tab}, $\rho^{'}$, l, and A are the electrical resistance, resistivity, length, and cross-section of the corresponding tab, respectively.

4.2. Description of the thermal methodology

Fig. 11 shows the thermal modeling methodology and coupling of 1D with 3D of an LTO cell which treats the battery as a core with two tabs. Using the Matlab/Simulink software the 1D electro-thermal model is used to find the reaction and polarization of the heat generation.

One of the common methods to study cell's temperature and voltage characteristics [70,71] is the coupling of a 1D electrochemical with a 3D thermal model. However, the electrochemical model [72] requires many
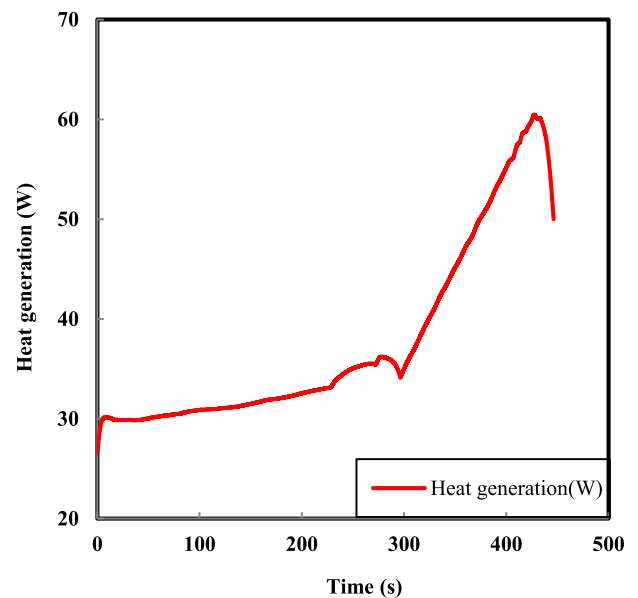

Fig. 12. The heat generation of the LTO cell in 8C discharging rate.

parameters which some of them need invasive and expensive methods to be achieved, such as the length of the electrode or the diffusivity coefficient. Hence, an electrical model is used instead of an electrochemical model to assess the heat generation estimation for 3D thermal modeling [68,73-75]. The heat generation value is placed in the COMSOL Multiphysics software as a heat source to calculate the heat distribution pattern. The heat generation of the cell in the 8C discharging rate at different times has been reported in Fig. 12. The time of 0 s represents the SOC 100% and the 446 s represents the SOC of 0%.

4.3. Validation of the thermal model

To validate the accuracy of the battery thermal model, the temperature variation measured from the experimental tests are compared with simulation results conducted with the COMSOL Multiphysics®. A 23Ah LTO battery cell is taken as a sample and discharge under 184A in four different scenarios. Totally eight thermocouples are set on the front and back sidewalls of the battery cell. With the purpose of the validation and
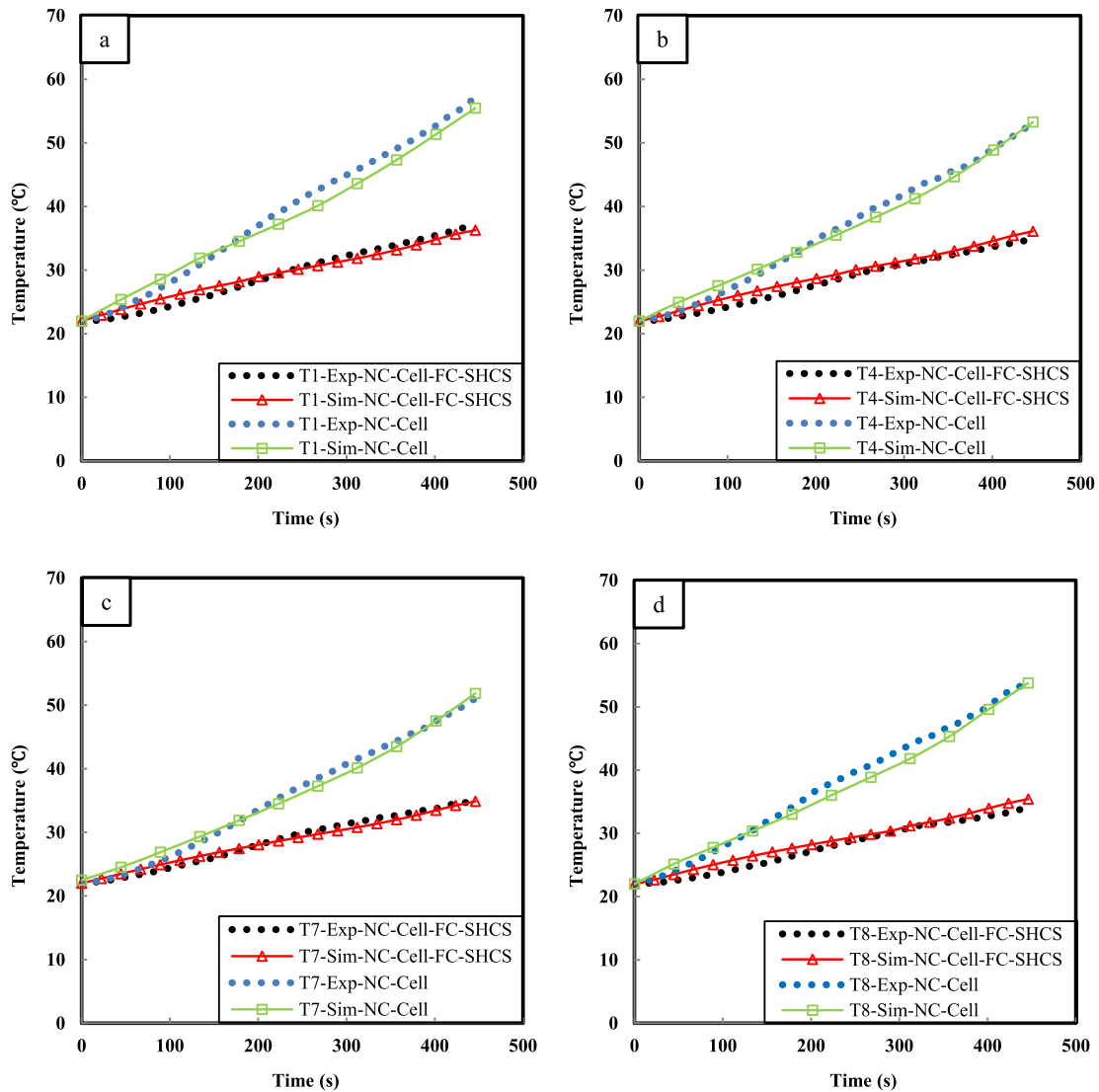
Fig. 13. Thermal model validation of natural (NC-Cell) and forced convection (NC-Cell-FC-SHCS) for (a) T_1, (b) T_4, (c) T_7 and (d) T_8 in the 8C discharging rate (Sim: Simulation).

show the accuracy of the numerical method, the temperatures of thermocouples of T_1, T_4, T_7, and T_8 for the first and third scenarios during discharging mode are compared with the simulation results. The locations of thermocouples on the cell surface for both scenarios are shown in Fig. 3 and Fig. 6 respectively. As shown in Fig. 13, there is an adequate agreement by the comparison of the transient wall temperatures of simulation and experimental data for natural and forced convection during the discharge process. The precision of the numerical simulations lays the basis for the prediction of the thermal behavior of the cell in different boundary conditions.

4.4. Boundary condition and mesh grid independency

The initial temperature of the battery cells, SHCS, and the coolant are set to 22 °C. Moreover, coolant inlet velocity is turbulent in which the inlet velocity of the coolant is set to 3 m/s, and the outlet is assumed as the ambient pressure. The heat transfer through radiation is assumed to be negligible. The 3D thermal model is developed and solved numerically by COMSOL Multiphysics® using the heat transfer module of a commercial finite element solver, which is computed using the GMRES solver for the governing equations. Besides, the grid-independent test is performed to refine the grid number while the results are not influenced

by further refinement of the mesh, and the results error is kept within 5% [76].

Fig. 14 displays the maximum simulated temperature of the cell to estimate the independence of the grid number. The result differs only 1.5% when the grid number varies from 746,929 to 1,246,482. Consequently, owing to computational time-saving, the grid number of 746,929 is chosen for the cell simulation.

4.5. Simulation results and discussion

4.5.1. The natural and forced convection cooling effect in cell level

For the thermal model, the validation tests are done with discharging at a high constant current of 184A from 100% to 0% of SOC. Consistent with the thermal image at an ambient temperature of 22 °C shown in Fig. 5, there is a hot zone in the middle and on top of the cell. Therefore, a computationally efficient localized heat source model has been implemented in the cell domain in order to simulate the non-uniform temperature distribution through the cell domain [77]. Fig. 15a shows the heat distribution and maximum temperature in simulation which is very close to the experimental test and thermal images. Moreover, based on Fig. 13 the transient simulation for natural convection is in good agreement with measured transient wall cell surface temperature.
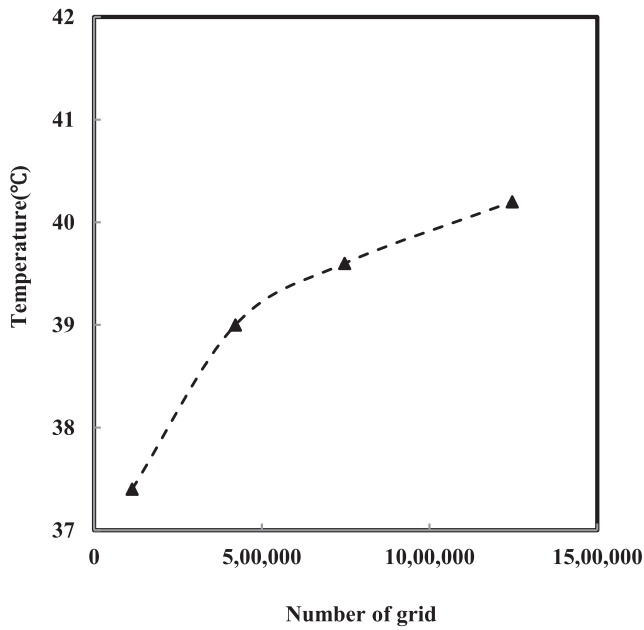
Fig. 14. Grid number independency test.

Fig. 15b,c shows the temperature and velocity transient simulation of the cell equipped with the SHCS when the cell and heat pipes condenser are under natural and forced convection respectively. As it is obvious in Fig. 15c the temperatures of condensers reduce from the nearest plane to the evaporator until the end of the condenser. Forced convection with an
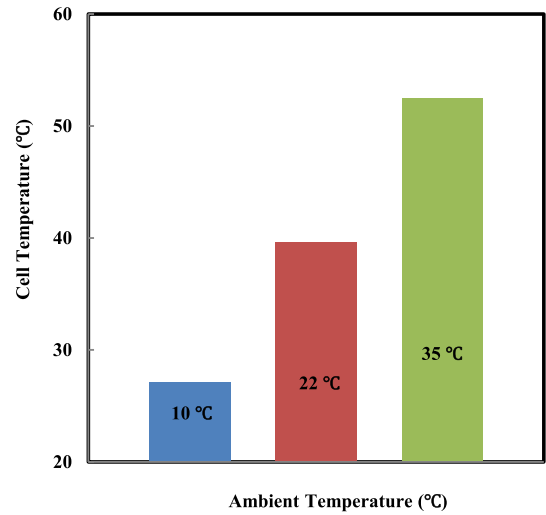

Fig. 16. The temperature of the cell in different ambient temperatures with an inlet velocity of 3 m/s in the 8C (184A) discharging rate (446 s).
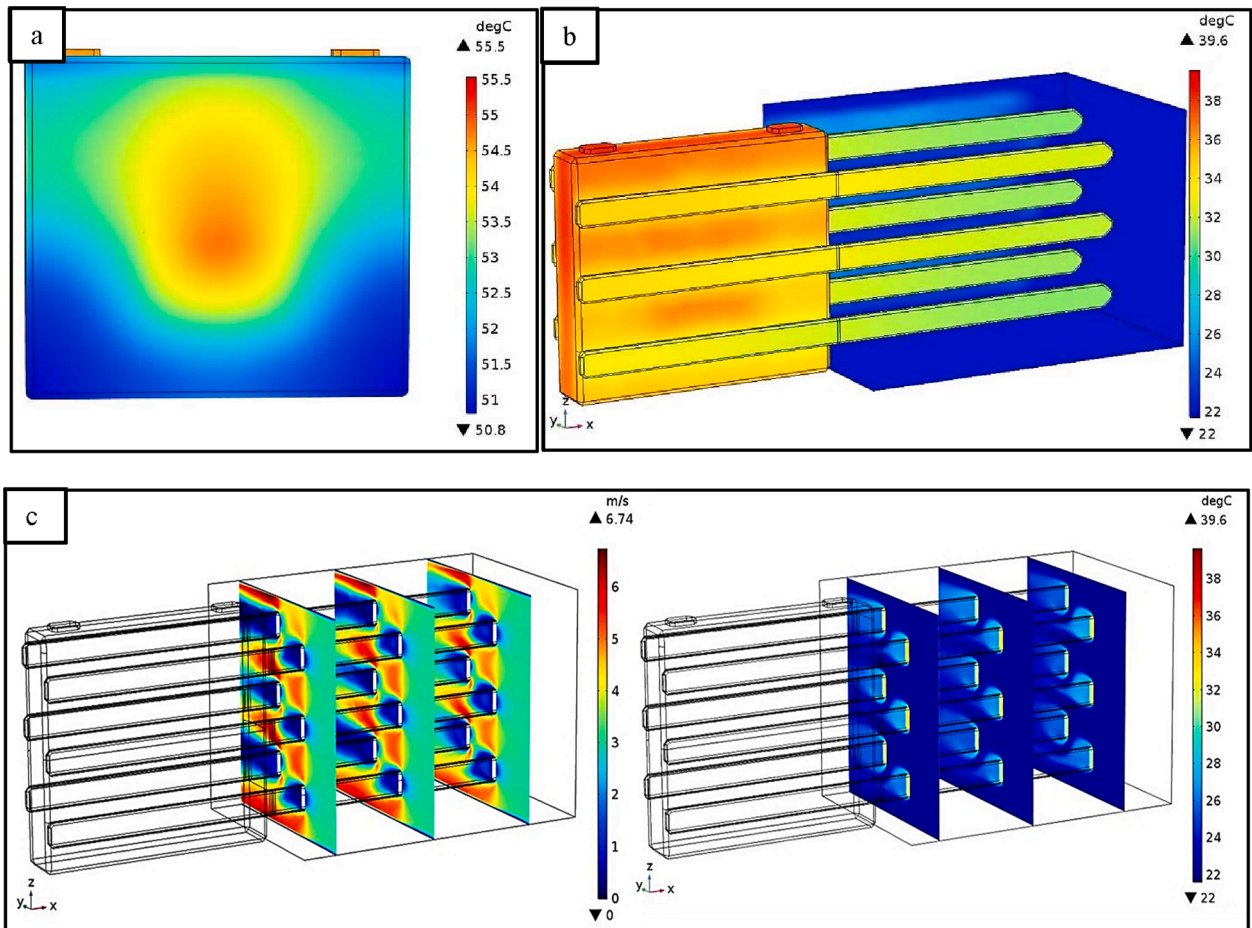

Fig. 15. (a) Temperature contour of the LTO cell in natural convection (NC-Cell), (b) cell embedded with SHCS (NC-Cell-FC-SHCS) in forced convection, and (c) velocity and temperature surface contour of cell embedded with SHCS (NC-Cell-FC-SHCS) in forced convection with an inlet velocity of 3 m/s in the 8C(184A) discharging rate(446 s).
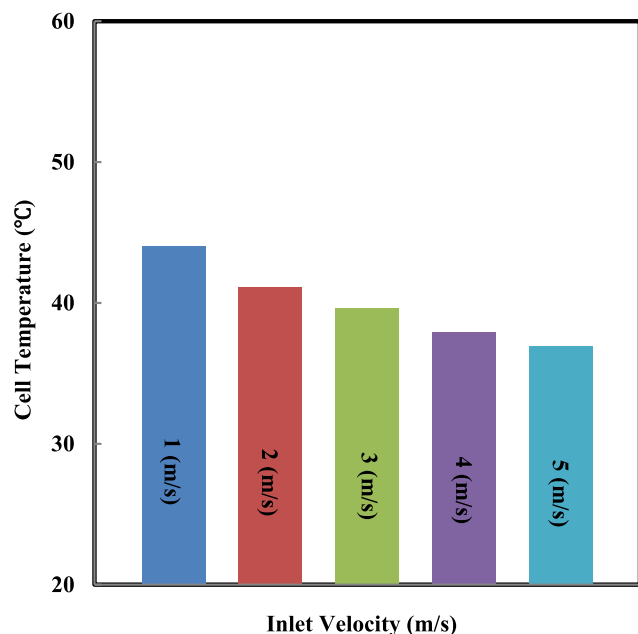
Fig. 17. The temperature of the cell in different inlet velocity with an ambient temperature of 22 °C in the 8C (184A) discharging rate (446 s).

inlet velocity of 3 m/s crosses the heat pipe condenser and efficiently takes away the heat from the single cell. Such excellent agreements in transient response in cell level (Fig. 13) propose that the model can predict the transient thermal performance reasonably well and can be further applied to the study of the thermal performance of SHCS for different boundary conditions. It is important to note that in current study the heat pipe is replaced by a solid region, and the effective thermal conductivity of components is used in the simulation [43,50,77-79].

4.5.2. Forced convection approach in different ambient temperatures for cell level

Ambient temperature has a direct effect on battery power, decay rate, and capacity. Consequently, it is vital to consider the performance of Li-ion cell under different temperature conditions. In the following section, the temperature of LTO cell embedded with SHCS in the 8C discharging rate and three different ambient temperatures, including 10 °C, 22 °C, and 35 °C are investigated. It is obvious that the ambient temperature of the air considerably impacts the temperature of the cell. Fig. 16 shows the ambient temperatures of 10 °C, 22 °C, and 35 °C result in 27.1 °C, 39.6 °C and 52.5 °C temperature of the cell respectively.

4.5.3. Forced convection approach in different inlet velocity for cell level

Fig. 17 displays the results of the temperature and inlet velocity from the CFD analysis using the baseline conditions. As the inlet velocity is increased, the convective heat transfer on the cell is estimated to be improved, consequently, the cell temperature is reduced nevertheless at the higher pressure drop or pumping power. By setting the inlet air velocity to 1 m/s, 2 m/s, 3 m/s, 4 m/s and 5 m/s the maximum temperature evolution reach 44 °C, 41.1 °C, 39.6 °C, 37.9 °C and 36.9 °C, respectively. It can be seen that by increasing the air velocity, the cell temperature reduces. Therefore, there is an opposite relationship between the inlet velocity and the maximum temperature of the cell.

5. Conclusion

Heat generation is one of the main factors in battery cell aging, safety, and capacity. The temperature inhomogeneity results in imbalanced aging and leads to the degradation of the cell performance. In order to avoid such undesirable behaviors, a developed TMS is necessary at the cell/module level. In this paper, SHCS is suggested for the high current discharging of the LTO battery cell. Surface temperature histories and temperature gradients of the LTO cell are collected experimentally and compared in four cooling scenarios. In the first scenario, the temperature of the cell is considered in natural convection. In the second to fourth scenarios, the effect of SHCS is investigated in natural and forced convection to improve the cooling performance. It was found that the maximum cell temperature embedded with SCHS for natural convection, forced convection for SHCS, and forced convection for cell and SHCS reduce the cell temperature by 13.7%, 31.6%, and 33.4% respectively. Moreover, A CFD model is employed to investigate the thermal performance of the SHCS under different transient boundary conditions.

Future work

In the current study, the effect of the SHCS and air cooling system has been considered experimentally and numerically on Li-ion battery temperature. Future work will be focused on the optimization of the battery module/pack with SHCS in different boundary conditions. Besides, using wet cooling/evaporative cooling is an option to increase the efficiency of the cooling system.

Declaration of Competing Interest

The authors declared that there is no conflict of interest.

Acknowledgment

References

[1] M. Lu, X. Zhang, J. Ji, X. Xu, Y. Zhang, Research progress on power battery cooling technology for electric vehicles, J. Energy Storage. 27 (2020), 101155, https://doi.org/10.1016/J.EST.2019.101155.

[2] W. Yang, F. Zhou, H. Zhou, Q. Wang, J. Kong, Thermal performance of cylindrical Lithium-ion battery thermal management system integrated with mini-channel liquid cooling and air cooling, Appl. Therm. Eng. (2020), 115331, https://doi.org/10.1016/J.APPLTHERMALENG.2020.115331.

[3] S.K. Mohammadian, Y. Zhang, Thermal management optimization of an air-cooled Li-ion battery module using pin-fin heat sinks for hybrid electric vehicles, J. Power Sources 273 (2015) 431–439, https://doi.org/10.1016/J.JPOWSOUR.2014.09.110.

[4] Z. Zhang, K. Wei, Experimental and numerical study of a passive thermal management system using flat heat pipes for lithium-ion batteries, Appl. Therm. Eng. 166 (2020), 114660, https://doi.org/10.1016/J.APPLTHERMALENG.2019.114660.

[5] L.H. Saw, H.M. Poon, H.S. Thiam, Z. Cai, W.T. Chong, N.A. Pambudi, Y.J. King, Novel thermal management system using mist cooling for lithium-ion battery packs, Appl. Energy 223 (2018) 146–158, https://doi.org/10.1016/J.APENERGY.2018.04.042.

[6] J. Sun, J. Li, T. Zhou, K. Yang, S. Wei, N. Tang, N. Dang, H. Li, X. Qiu, L. Chen, Toxicity, a serious concern of thermal runaway from commercial Li-ion battery, Nano Energy 27 (2016) 313–319, https://doi.org/10.1016/J.NANOEN.2016.06.031.

[7] Q. Wang, B. Jiang, B. Li, Y. Yan, A critical review of thermal management models and solutions of lithium-ion batteries for the development of pure electric vehicles, Renew. Sustain. Energy Rev. 64 (2016) 106–128, https://doi.org/10.1016/J.RSER.2016.05.033.

[8] Á.G. Miranda, C.W. Hong, Integrated modeling for the cyclic behavior of high power Li-ion batteries under extended operating conditions, Appl. Energy 111 (2013) 681–689, https://doi.org/10.1016/J.APENERGY.2013.05.047.

[9] Y. Ye, Y. Shi, A.A.O. Tay, Electro-thermal cycle life model for lithium iron phosphate battery, J. Power Sources 217 (2012) 509–518, https://doi.org/10.1016/J.JPOWSOUR.2012.06.055.

[10] A.A. Pesaran, Battery thermal models for hybrid vehicle simulations, J. Power Sources 110 (2002) 377–382, https://doi.org/10.1016/S0378-7753(02)00200-8.

[11] T.M. Bandhauer, S. Garimella, T.F. Fuller, A critical review of thermal issues in lithium-ion batteries, J. Electrochem. Soc. 158 (2011), https://doi.org/10.1149/1.3515880.

[12] L.H. Saw, Y. Ye, A.A.O. Tay, W.T. Chong, S.H. Kuan, M.C. Yew, Computational fluid dynamic and thermal analysis of Lithium-ion battery pack with air cooling, Appl. Energy 177 (2016) 783–792, https://doi.org/10.1016/j.apenergy.2016.05.122.

[13] R. Kizilel, R. Sabbah, J.R. Selman, S. Al-Hallaj, An alternative cooling system to enhance the safety of Li-ion battery packs, J. Power Sources 194 (2009) 1105–1112, https://doi.org/10.1016/J.JPOWSOUR.2009.06.074.

[14] L.H. Saw, Y. Ye, M.C. Yew, W.T. Chong, M.K. Yew, T.C. Ng, Computational fluid dynamics simulation on open cell aluminium foams for Li-ion battery cooling system, Appl. Energy 204 (2017) 1489–1499, https://doi.org/10.1016/J.APENERGY.2017.04.022.

[15] A. Jarrett, I.Y. Kim, Design optimization of electric vehicle battery cooling plates for thermal performance, J. Power Sources 196 (2011) 10359–10368, https://doi.org/10.1016/J.JPOWSOUR.2011.06.090.

[16] H. Park, A design of air flow configuration for cooling lithium ion battery in hybrid electric vehicles, J. Power Sources 239 (2013) 30–36, https://doi.org/10.1016/J.JPOWSOUR.2013.03.102.

[17] M. Safdari, R. Ahmadi, S. Sadeghzadeh, Numerical investigation on PCM encapsulation shape used in the passive-active battery thermal management, Energy. 193 (2020), 116840, https://doi.org/10.1016/J.ENERGY.2019.116840.

[18] Z. Sun, R. Fan, F. Yan, T. Zhou, N. Zheng, Thermal management of the lithium-ion battery by the composite PCM-Fin structures, Int. J. Heat Mass Transf. 145 (2019), 118739, https://doi.org/10.1016/J.IJHEATMASSTRANSFER.2019.118739.

[19] K. Chen, Y. Chen, Y. She, M. Song, S. Wang, L. Chen, Construction of effective symmetrical air-cooled system for battery thermal management, Appl. Therm. Eng. 166 (2020), 114679, https://doi.org/10.1016/J.APPLTHERMALENG.2019.114679.

[20] J. Cao, Z. Ling, X. Fang, Z. Zhang, Delayed liquid cooling strategy with phase change material to achieve high temperature uniformity of Li-ion battery under high-rate discharge, J. Power Sources 450 (2020), 227673, https://doi.org/10.1016/J.JPOWSOUR.2019.227673.

[21] D. Karimi, H. Behi, J. Jaguemont, M. El Baghdadi, J. Van Mierlo, O. Hegazy, Thermal Concept Design of MOSFET Power Modules in Inverter Subsystems for Electric Vehicles, (2019).

[22] M. Behi, S.A. Mirmohammadi, M. Ghanbarpour, H. Behi, B. Palm, Evaluation of a novel solar driven sorption cooling/heating system integrated with PCM storage compartment, Energy. 164 (2018) 449–464, https://doi.org/10.1016/J.ENERGY.2018.08.166.

[23] Z. Liu, Y. Wang, J. Zhang, Z. Liu, Shortcut computation for the thermal management of a large air-cooled battery pack, Appl. Therm. Eng. 66 (2014) 445–452, https://doi.org/10.1016/J.APPLTHERMALENG.2014.02.040.

[24] K. Chen, W. Wu, F. Yuan, L. Chen, S. Wang, Cooling efficiency improvement of air-cooled battery thermal management system through designing the flow pattern, Energy. 167 (2019) 781–790, https://doi.org/10.1016/J.ENERGY.2018.11.011.

[25] X. Li, F. He, L. Ma, Thermal management of cylindrical batteries investigated using wind tunnel testing and computational fluid dynamics simulation, J. Power Sources 238 (2013) 395–402, https://doi.org/10.1016/J.JPOWSOUR.2013.04.073.

[26] R. Mahamud, C. Park, Reciprocating air flow for Li-ion battery thermal management to improve temperature uniformity, J. Power Sources 196 (2011) 5685–5696, https://doi.org/10.1016/j.jpowsour.2011.02.076.

[27] S. Pesaran, A., Keyser, M., and Burch, No Title, in: An Approach Des. Therm. Manag. Syst. Electr. Hybrid Veh. Batter. Packs, United States, 1999.

[28] H. Fathabadi, High thermal performance lithium-ion battery pack including hybrid active–passive thermal management system for using in hybrid/electric vehicles, Energy. 70 (2014) 529–538, https://doi.org/10.1016/J.ENERGY.2014.04.046.

[29] Z. Qian, Y. Li, Z. Rao, Thermal performance of lithium-ion battery thermal management system by using mini-channel cooling, Energy Convers. Manag. 126 (2016) 622–631, https://doi.org/10.1016/J.ENCONMAN.2016.08.063.

[30] S. Basu, K.S. Hariharan, S.M. Kolake, T. Song, D.K. Sohn, T. Yeo, Coupled electrochemical thermal modelling of a novel Li-ion battery pack thermal management system, Appl. Energy 181 (2016) 1–13, https://doi.org/10.1016/J.APENERGY.2016.08.049.

[31] F. Wu, Z. Rao, The lattice Boltzmann investigation of natural convection for nanofluid based battery thermal management, Appl. Therm. Eng. 115 (2017) 659–669, https://doi.org/10.1016/J.APPLTHERMALENG.2016.12.139.

[32] M.S. Patil, J.-H. Seo, S. Panchal, S.-W. Jee, M.-Y. Lee, Investigation on thermal performance of water-cooled Li-ion pouch cell and pack at high discharge rate with U-turn type microchannel cold plate, Int. J. Heat Mass Transf. 155 (2020), 119728, https://doi.org/10.1016/j.ijheatmasstransfer.2020.119728.

[33] H. Liu, Z. Wei, W. He, J. Zhao, Thermal issues about Li-ion batteries and recent progress in battery thermal management systems: A review, Energy Convers. Manag. 150 (2017) 304–330, https://doi.org/10.1016/J.ENCONMAN.2017.08.016.

[34] M. Behi, M. Shakorian-poor, S.A. Mirmohammadi, H. Behi, J.I. Rubio, N. Nikkam, M. Farzaneh-Gord, Y. Gan, M. Behnia, Experimental and numerical investigation on hydrothermal performance of nanofluids in micro-tubes, Energy. 193 (2020), 116658, https://doi.org/10.1016/J.ENERGY.2019.116658.

[35] S. Mirmohammadi, M. Behi, Investigation on Thermal Conductivity, Viscosity and Stability of Nanofluids (2012) 140.

[36] M.M. Heyhat, S. Mousavi, M. Siavashi, Battery thermal management with thermal energy storage composites of PCM, metal foam, fin and nanoparticle, J. Energy Storage. 28 (2020), 101235, https://doi.org/10.1016/J.EST.2020.101235.

[37] Z. Ling, J. Chen, X. Fang, Z. Zhang, T. Xu, X. Gao, S. Wang, Experimental and numerical investigation of the application of phase change materials in a simulative power batteries thermal management system, Appl. Energy 121 (2014) 104–113, https://doi.org/10.1016/J.APENERGY.2014.01.075.

[38] N. Javani, I. Dincer, G.F. Naterer, G.L. Rohrauer, Modeling of passive thermal management for electric vehicle battery packs with PCM between cells, Appl. Therm. Eng. 73 (2014) 307–316, https://doi.org/10.1016/j.applthermaleng.2014.07.037.

[39] N. Javani, I. Dincer, G.F. Naterer, B.S. Yilbas, Heat transfer and thermal management with PCMs in a Li-ion battery cell for electric vehicles, Int. J. Heat Mass Transf. 72 (2014) 690–703, https://doi.org/10.1016/j.ijheatmasstransfer.2013.12.076.

[40] R. Sabbah, R. Kizilel, J.R. Selman, S. Al-Hallaj, Active (air-cooled) vs. passive (phase change material) thermal management of high power lithium-ion packs: Limitation of temperature rise and uniformity of temperature distribution, J. Power Sources 182 (2008) 630–638, https://doi.org/10.1016/J.JPOWSOUR.2008.03.082.

[41] W. Wu, X. Yang, G. Zhang, K. Chen, S. Wang, Experimental investigation on the thermal performance of heat pipe-assisted phase change material based battery thermal management system, Energy Convers. Manag. 138 (2017) 486–492, https://doi.org/10.1016/J.ENCONMAN.2017.02.022.

[42] F. Samimi, A. Babapoor, M. Azizi, G. Karimi, Thermal management analysis of a Li-ion battery cell using phase change material loaded with carbon fibers, Energy. 96 (2016) 355–371, https://doi.org/10.1016/J.ENERGY.2015.12.064.

[43] H. Behi, Experimental and numerical study on heat pipe assisted PCM storage system, (2015).

[44] H. Behi, M. Ghanbarpour, M. Behi, Investigation of PCM-assisted heat pipe for electronic cooling, Appl. Therm. Eng. 127 (2017) 1132–1142, https://doi.org/10.1016/J.APPLTHERMALENG.2017.08.109.

[45] C.A. Chung, S.-W. Yang, C.-Y. Yang, C.-W. Hsu, P.-Y. Chiu, Experimental study on the hydrogen charge and discharge rates of metal hydride tanks using heat pipes to enhance heat transfer, Appl. Energy 103 (2013) 581–587, https://doi.org/10.1016/J.APENERGY.2012.10.024.

[46] Y.-C. Weng, H.-P. Cho, H.-C. Chang, S.-L. Chen, Heat pipe with PCM for electronic cooling, Appl. Energy 88 (2011) 1825–1833, https://doi.org/10.1016/J.APENERGY.2010.12.004.

[47] A. Faghri, Heat Pipe Science and Technology, Taylor & Francis., 1995.

[48] Y.F. Maydanik, S.V. Vershinin, Development and tests of ammonia Miniature Loop Heat Pipes with cylindrical evaporators, Appl. Therm. Eng. 29 (2009) 2297–2301, https://doi.org/10.1016/J.APPLTHERMALENG.2008.11.016.

[49] M.-S. Wu, K.H. Liu, Y.-Y. Wang, C.-C. Wan, Heat dissipation design for lithium-ion batteries, J. Power Sources 109 (2002) 160–166, https://doi.org/10.1016/S0378-7753(02)00048-4.

[50] H. Behi, D. Karimi, M. Behi, M. Ghanbarpour, J. Jaguemont, M. Akbarzadeh Sokkeh, F. Heidari Gandoman, M. Berecibar, J. Van Mierlo, A new concept of thermal management system in Li-ion battery using air cooling and heat pipe for electric vehicles, Appl. Therm. Eng. (2020), 115280, https://doi.org/10.1016/J.APPLTHERMALENG.2020.115280.

[51] D. Dan, C. Yao, Y. Zhang, H. Zhang, Z. Zeng, X. Xu, Dynamic thermal behavior of micro heat pipe array-air cooling battery thermal management system based on thermal network model, Appl. Therm. Eng. 162 (2019), 114183, https://doi.org/10.1016/J.APPLTHERMALENG.2019.114183.

[52] X. Ye, Y. Zhao, Z. Quan, Experimental study on heat dissipation for lithium-ion battery based on micro heat pipe array (MHPA), Appl. Therm. Eng. 130 (2018) 74–82, https://doi.org/10.1016/j.applthermaleng.2017.10.141.

[53] Y. Ye, L.H. Saw, Y. Shi, A.A.O. Tay, Numerical analyses on optimizing a heat pipe thermal management system for lithium-ion batteries during fast charging, Appl. Therm. Eng. 86 (2015) 281–291, https://doi.org/10.1016/J.APPLTHERMALENG.2015.04.066.

[54] T.-H. Tran, S. Harmand, B. Desmet, S. Filangi, Experimental investigation on the feasibility of heat pipe cooling for HEV/EV lithium-ion battery, Appl. Therm. Eng. 63 (2014) 551–558, https://doi.org/10.1016/J.APPLTHERMALENG.2013.11.048.

[55] A. Samba, N. Omar, H. Gualous, Y. Firouz, P. Van den Bossche, J. Van Mierlo, T. I. Boubekeur, Development of an Advanced Two-Dimensional Thermal Model for Large size Lithium-ion Pouch Cells, Electrochim. Acta 117 (2014) 246–254, https://doi.org/10.1016/J.ELECTACTA.2013.11.113.

[56] W. Zhao, G. Luo, C.-Y. Wang, Effect of tab design on large-format Li-ion cell performance, J. Power Sources 257 (2014) 70–79, https://doi.org/10.1016/J.JPOWSOUR.2013.12.146.

[57] A. Eddahech, O. Briat, J.-M. Vinassa, Thermal characterization of a high-power lithium-ion battery: Potentiometric and calorimetric measurement of entropy changes, Energy. 61 (2013) 432–439, https://doi.org/10.1016/J.ENERGY.2013.09.028.

[58] J.B. Robinson, J.A. Darr, D.S. Eastwood, G. Hinds, P.D. Lee, P.R. Shearing, O. O. Taiwo, D.J.L. Brett, Non-uniform temperature distribution in Li-ion batteries during discharge – A combined thermal imaging, X-ray micro-tomography and electrochemical impedance approach, J. Power Sources 252 (2014) 51–57, https://doi.org/10.1016/J.JPOWSOUR.2013.11.059.

[59] C. Veth, D. Dragicevic, C. Merten, Thermal characterizations of a large-format lithium ion cell focused on high current discharges, J. Power Sources 267 (2014) 760–769, https://doi.org/10.1016/J.JPOWSOUR.2014.05.139.

[60] S. Panchal, S. Mathewson, R. Fraser, R. Culham, M. Fowler, Measurement of Temperature Gradient (dT/dy) and Temperature Response (dT/dt) of a Prismatic Lithium-Ion Pouch Cell with LiFePO4 Cathode Material, in: WCXTM 17 SAE World Congr. Exp., SAE International, 2017. doi:https://doi.org/10.4271/2017-01-1207.

[61] S. Goutam, J. Timmermans, N. Omar, P. Van Den Bossche, J. Van Mierlo, L. Rodriguez, N. Nieto, M. Swierczynski, Surface temperature evolution and the

location of maximum and average surface temperature of a lithium-ion pouch cell under variable load profiles, Euroepan Electr. Veh. Congr. (2014) 1–7.

[62] M. Sheikholeslami, D.D. Ganji, Heat transfer improvement in a double pipe heat exchanger by means of perforated turbulators, Energy Convers. Manag. 127 (2016) 112–123, https://doi.org/10.1016/J.ENCONMAN.2016.08.090.

[63] M. Sheikholeslami, D.D. Ganji, Heat transfer enhancement in an air to water heat exchanger with discontinuous helical turbulators; experimental and numerical studies, Energy. 116 (2016) 341–352, https://doi.org/10.1016/J.ENERGY.2016.09.120.

[64] Z. Li, J. Zhang, B. Wu, J. Huang, Z. Nie, Y. Sun, F. An, N. Wu, Examining temporal and spatial variations of internal temperature in large-format laminated battery with embedded thermocouples, J. Power Sources 241 (2013) 536–553, https://doi.org/10.1016/J.JPOWSOUR.2013.04.117.

[65] S. Goutam, J.M. Timmermans, N. Omar, P. Van den Bossche, J. Van Mierlo, Comparative study of surface temperature behavior of commercial li-ion pouch cells of different chemistries and capacities by infrared thermography, Energies. 8 (2015) 8175–8192, https://doi.org/10.3390/en8088175.

[66] P. Van den Bossche, N. Omar, M. Al Sakka, A. Samba, H. Gualous, J. Van Mierlo, The Challenge of PHEV Battery Design and the Opportunities of Electrothermal Modeling, Lithium-Ion Batter. (2014) 249–271, https://doi.org/10.1016/B978-0-444-59513-3.00011-X.

[67] M. Soltani, G. Berckmans, J. Jaguemont, J. Ronsmans, S. Kakihara, O. Hegazy, J. Van Mierlo, N. Omar, Three dimensional thermal model development and validation for lithium-ion capacitor module including air-cooling system, Appl. Therm. Eng. 153 (2019) 264–274, https://doi.org/10.1016/j.applthermaleng.2019.03.023.

[68] J. Goutam, L. Boulon, Y. Dubé, Characterization and modeling of a hybrid-electric-vehicle lithium-ion battery pack at low temperatures, IEEE Trans. Veh. Technol. 65 (2016) 1–14, https://doi.org/10.1109/TVT.2015.2391053.

[69] M. Soltani, J. Ronsmans, J. Jaguemont, J. Van Mierlo, P. Van Den Bossche, N. Omar, A Three-dimensional thermal model for a commercial lithium-ion capacitor battery pack with non-uniform temperature distribution, Proc. IEEE Int. Conf. Ind. Technol. (2019) 1126–1131, https://doi.org/10.1109/ICIT.2019.8755081.

[70] I.B.; O.B.; A.E.; J.M.V.; I.B.; P. Gyan, Electro-thermal model of lithium-ion batteries for electrified vehicles applications, 2015 IEEE 24th Int. Symp. Ind. Electron. (ISIE), Buzios, 2015, Pp. 1248-1252. (n.d.).

[71] T.C. and J.V.M. Noshin Omar *, Peter Van den Bossche, Peukert Revisited—Critical Appraisal and Need for Modification for Lithium-Ion Batteries, Energies 2013, 6, 5625-5641. (n.d.).

[72] J. Jaguemont, L. Boulon, Y. Dubé, A comprehensive review of lithium-ion batteries used in hybrid and electric vehicles at cold temperatures, Appl. Energy 164 (2016) 99–114, https://doi.org/10.1016/J.APENERGY.2015.11.034.

[73] J. Jaguemont, D. Karimi, J. Van Mierlo, Optimal passive thermal management of lithium-ion capacitors for automotive applications (2019) 1–8.

[74] Y.D. and F.M. J. Jaguemont, L. Boulon, Thermal Management of a Hybrid Electric Vehicle in Cold Weather, IEEE Trans. Energy Conversion, Vol. 31, No. 3, Pp. 1110-1120, Sept. 2016. (n.d.).

[75] J. Jaguemont, N. Omar, M. Abdel-Monem, P. Van den Bossche, J. Van Mierlo, Fast-charging investigation on high-power and high-energy density pouch cells with 3D-thermal model development, Appl. Therm. Eng. 128 (2018) 1282–1296, https://doi.org/10.1016/J.APPLTHERMALENG.2017.09.068.

[76] Y. Ye, Y. Shi, L.H. Saw, A.A.O. Tay, Performance assessment and optimization of a heat pipe thermal management system for fast charging lithium ion battery packs, Int. J. Heat Mass Transf. 92 (2016) 893–903, https://doi.org/10.1016/J.IJHEATMASSTRANSFER.2015.09.052.

[77] H. Behi, D. Karimi, M. Behi, J. Jaguemont, M. Ghanbarpour, M. Behnia, M. Berecibar, J. Van Mierlo, Thermal management analysis using heat pipe in the high current discharging of lithium-ion battery in electric vehicles, J. Energy Storage. 32 (2020), 101893, https://doi.org/10.1016/j.est.2020.101893.

[78] M. Ghanbarpour, R. Khodabandeh, Entropy generation analysis of cylindrical heat pipe using nanofluid, Thermochim Acta 610 (2015) 37–46, https://doi.org/10.1016/j.tca.2015.04.028.

[79] M.H.A. Elnaggar, M.Z. Abdullah, S. Raj, R. Munusamy, Experimental and Numerical Studies of Finned L-Shape Heat Pipe for Notebook-PC Cooling, IEEE Trans. Components, Packag. Manuf. Technol. 3 (2013) 978–988, https://doi.org/10.1109/TCPMT.2013.2245944.

[80] Danial Karimi, et al., Thermal performance enhancement of phase change material using aluminum-mesh grid foil for lithium-capacitor modules, J. Energy Storage 30 (101508) (2020), https://doi.org/10.1016/j.est.2020.101508 (in press).

[81] Foad Heidari Gandoman, et al., Reliability evaluation of Li-ion batteries for electric vehicles applications from the thermal perspectives. Uncertainties in Modern Power Systems 1st, 1, Elsevier, 2020, pp. 564–578, 9780128204917 (in press).